REVIEWS

High temperature magnetic semiconductors: narrow band gaps and two-dimensional systems

Bo Gu[1, 2, †]

[1]Kavli Institute for Theoretical Sciences, and CAS Center for Excellence in Topological Quantum Computation, University of Chinese Academy of Sciences, Beijing 100190, China

[2]Physical Science Laboratory, Huairou National Comprehensive Science Center, Beijing 101400, China

Abstract: Magnetic semiconductors have been demonstrated to work at low temperatures, but not yet at room temperature for spin electronic applications. In contrast to the p-type diluted magnetic semiconductors, n-type diluted magnetic semiconductors are few. Using a combined method of the density function theory and quantum Monte Carlo simulation, we briefly discuss the recent progress to obtain diluted magnetic semiconductors with both p- and n-type carriers by choosing host semiconductors with a narrow band gap. In addition, the recent progress on two-dimensional intrinsic magnetic semiconductors with possible room temperature ferromangetism and quantum anomalous Hall effect are also discussed.

Key words: magnetic semiconductor; narrow band gap; two dimensional systems

1. Introduction

Spin electronics is a rapidly developing interdisciplinary subject in condensed matter physics. Electrons have two intrinsic properties: charge and spin. Traditional electronic devices, through the regulation of electronic charge to achieve a variety of functions, with the continuous enhancement of performance, the size of the device is decreasing, has been close to the physical limit of atomic scale. In order to surpass the traditional electronic devices, the research on how to regulate the spin electronics of electron spin has been developed gradually, and many novel physical phenomena and new materials have been produced, such as giant magnetoresistance, tunnel magnetoresistance, magnetic semiconductor, spin Hall effect, quantum spin Hall effect, quantum anomalous Hall effect, topological insulator, etc.[1, 2].

The development history of condensed matter physics shows that the in-depth study of novel physical phenomena is helpful to deepen our understanding of condensed state physics and expand the boundary of condensed matter physics. It is of great significance in basic science and practical application. A typical example is giant magnetoresistance discovered in the 1988, which, with the deepening of research, has triggered the revolution of large capacity and miniaturization of hard disks. It has been widely used in high-density readout head and magnetic storage elements, and has become the standard technology of computer hard disks. However, many novel physical phenomena in spin electronics have not been applied in practice at present. An important constraint is that some novel physical phenomena are observed only at low temperatures in the laboratory, and the practical application requires that such physical phenomena can be realized at room temperature.

An important material is the magnetic semiconductor, which urgently needs to improve the temperature of its realization. Magnetic semiconductors, which combine the two important areas of magnetism and semiconductors, have been widely studied and are a basic material for the realization of spin electronics devices. The practical application requires that the ferromagnetic Curie temperature of magnetic semiconductors be higher than that of room temperature. Can we create magnetic semiconductors that work at room temperature? It is one of the 125 unknown scientific problems listed by Science in 2005[3]. Although some research articles claim to have been experimentally obtained for ferromagnetic semiconductors at room temperature, so far, room temperature ferromagnetic semiconductors, which have been widely repeated and widely accepted, have not been obtained yet.

The most extensive and in-depth study of magnetic semiconductor materials is (Ga,Mn)As[4, 5]. The present record of its Curie temperature T_c is about 200 K, which was created in 2011 by Institute of Semiconductors in Chinese Academy of Sciences[6]. A lot of difficulties have been encountered when trying to raise the Curie temperature of (Ga,Mn)As. The binary Mn ion is replaced with the trivalent Ga ion, and the magnetic moment and the hole carrier are introduced at the same time. Therefore, (Ga,Mn)As as a p-type magnetic semiconductor. The mismatch of the valence of manganese and gallium ions leads to severe and limited chemical solubility for the Mn in GaAs. In addition, because of the simultaneous doping of carriers and magnetic moments, it is difficult to turn the charge carriers and magnetism to its optimized condition separately. Therefore, there is an urgent need for new ideas and materials to explore room temperature magnetic semiconductors.

In order to solve the above difficulties, Li(Zn,Mn)As, regarded as I–II–V magnetic semiconductor, was proposed in the calculation[7], and later manufactured in the experiment
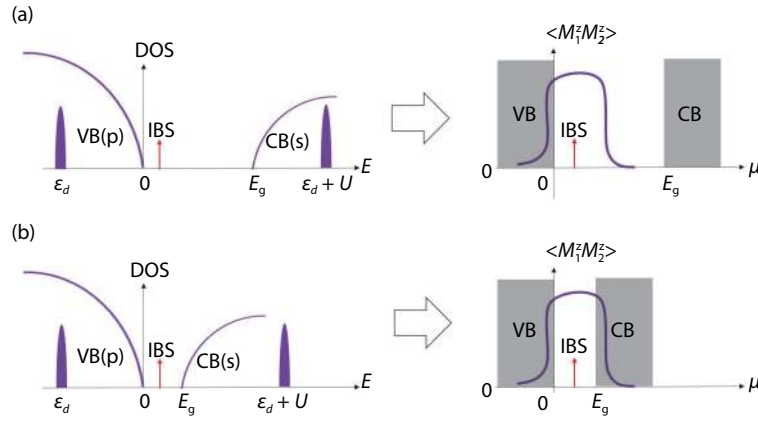
Fig. 1. (Color online) Schematic pictures of magnetic semiconductors with (a) wide band gaps and (b) narrow band gaps. The band gap is E_g. The top of valence band (VB) is dominated by p orbitals, and the bottom of conduction band (CB) is dominated by s orbitals. For the impurity with d orbitals, ε_d is impurity level of d orbitals, and U is the on-site Coulomb interaction. Impurity bound state (IBS) is also developed due to the doping of impurity into the host. The density of state (DOS) as a function of energy, and the magnetic correlation $\langle M_1^z M_2^z \rangle$ between two impurities as a function of the chemical potential μ are depicted. (a) Due to strong mixing between the impurity and the VB, the position of the IBS ω_{IBS} (arrow) is close to the top of the VB. Due to weak mixing between the impurity and the CB, usually no IBS appears below the bottom of the CB[19–21]. Thus, we have $0 \lesssim \omega_{\mathrm{IBS}} \ll E_g$ for the wide band gap case. By the condition $\mu \sim \omega_{\mathrm{IBS}}$, positive (FM coupling) $\langle M_1^z M_2^z \rangle$ can develop[22–24]. For p-type carriers ($\mu \sim 0$), ferromagnetic coupling can be obtained as the condition $\mu \sim \omega_{\mathrm{IBS}}$ can be satisfied. For n-type carriers ($\mu \sim E_g$), no magnetic coupling is obtained between impurities because the condition $\mu \sim \omega_{\mathrm{IBS}}$ cannot be satisfied[19–21]. (b) Case for narrow band gap E_g. By choosing suitable host semiconductors and impurities, the condition $0 \lesssim \omega_{\mathrm{IBS}} \lesssim E_g$ can be obtained. For both p-type and n-type carriers, ferromagnetic coupling can be obtained because the condition $\mu \sim \omega_{\mathrm{IBS}}$ is satisfied.

with $T_c = 50$ K[8]. By isovalent (Zn^{2+}, Mn^{2+}) substitution, spin is introduced. By tuning excess or deficient Li concentration, the carrier can be controlled independently. Although Li(Zn,Mn)As with excess Li^+ is considered to be a promising n-type magnetic semiconductor, p-type carriers were obtained in the experiment. The introduction of the hole is probably due to the excess Li^+ in substitutional Zn^{2+} sites[8]. In Li(Zn,Mn)P, another I–II–V magnetic semiconductor, $T_c = 34$ K is obtained in the experiment[9]. In the experiment, Li(Zn,Mn)P with excess Li was also identified as p-type, due to the same reason as that for Li(Zn,Mn)As[9]. A 1111-type magnetic semiconductor $(La_{1-x}Ba_x)(Zn_{1-x}Mn_x)AsO$ was reported with $T_c = 40$ K in the experiment [10]. Although these p-type magnetic semiconductors have some obvious advantages over (Ga,Mn)As, the obtained T_c is much lower than that of (Ga,Mn)As.

The T_c up to 230 K was achieved in another type of magnetic semiconductor $(Ba,K)(Zn,Mn)_2As_2$, which was created by the experimental group in Institute of Physics in Chinese Academy of Sciences in 2013[11, 12]. The magnetic moment is doped with isovalent (Zn^{2+}, Mn^{2+}) substitutions, and p-type carriers is introduced by (Ba^{2+}, K^+) substitutions. Driven by high T_c, the density functional theory calculations[13] and photoemission spectroscopy experiments [14, 15] were conducted to understand the mechanism of ferromagnetism in p-type $(Ba,K)(Zn,Mn)_2As_2$.

The evidence of n-type ferromagnetic semiconductor was obtained in the Co doped semiconductor $Ba(Zn,Co)_2As_2$ with Curie temperature of 45 K fabricated by the experimental group of Zhejiang University in 2019[16]. Both n-type carriers and spins are introduced due to the doping of Co.

Inspired by the above experimental progress, we proposed a new direction to obtain high temperature magnetic semiconductor by considering the magnetic semiconductors with narrow band gaps in 2016[17, 18]. Unlike the wide band gap magnetic semiconductors represented by (Ga,Mn) as, which have been studied extensively over the past 20 years, our calculations show that narrow band gap semiconductors are more likely to host both p- and n-type magnetic semiconductors. Because narrow band gap semiconductor is favored to form the shallow impurity levels, which is extended and can mediate ferromagnetic coupling between magnetic impurities in both p- and n-type carriers. The high Curie temperatures can also be expected due to long-range ferromagnetic coupling.

A schematic diagram describing magnetic semiconductors with wide band gap is shown in Fig. 1(a). In the studies of magnetic semiconductors with wide band gap E_g, such as (Zn,Mn)O[19], (Ga,Mn)As[20], and Mg(O,N)[21], the impurity bound state (IBS) ω_{IBS} was obtained close to the top of the valence band (VB), and usually no IBS is obtained below the bottom of the conduction band (CB). The ferromagnetic correlation (positive) $\langle M_1^z M_2^z \rangle$ between two impurities can be obtained when the chemical potential μ and IBS satisfy the relation $\mu \sim \omega_{\mathrm{IBS}}$[22, 23, 24]. For p-type carriers ($\mu \sim 0$), such relation can be satisfied, and the ferromagnetic coupling is obtained. For n-type carriers ($\mu \sim E_g$), such relation cannot be satisfied, and no magnetic coupling is obtained.

The situation changes for the magnetic semiconductors with narrow band gaps, as shown in Fig. 1(b). After selecting suitable host semiconductors and impurities, the relation $0 \lesssim \omega_{\mathrm{IBS}} \lesssim E_g$ can be obtained. As a result, for both the p- and the n-type carriers, the condition $\mu \sim \omega_{\mathrm{IBS}}$ is satisfied, and the ferromagnetic coupling can be expected.

Another possible direction to obtain high temperature magnetic semiconductors is van der Waals two-dimensional (2D) magnetic semiconductors. In 2017, Ising-type ferromagnet-

ism was observed in monolayer CrI$_3$ in experiment with Curie temperature T_c = 45 K[25]. In the same year, 2D magnetic semiconductor Cr$_2$Ge$_2$Te$_6$ was obtained in experiment with T_c = 28 K[26]. In 2018, two experimental teams declared that the single-layers VSe$_2$[27] and MnSe$_2$[28] have the Curie temperatures higher than room temperature.

In the following, we introduce our combined method of the density function theory and quantum Monte Carlo simulation (DFT + QMC). It was applied to study the magnetic semiconductors. For the cases with wide band gaps, Mn-doped ZnO and N-doped MgO are discussed. For the cases with narrow band gaps, Mn- and Cr-doped BaZn$_2$As$_2$ are discussed. In addition, the recently growing 2D magnetic semiconductors are also mentioned.

2. DFT + QMC method

There are two kinds of objects in magnetic semiconductors: one is the itinerant carriers, the other is the localized impurities. The itinerant carriers, which experience the periodic crystal potential and give rise to a *k*-dependent energy (i.e., electronic band structure), can be reasonably described by the mean-field theory, such as the density functional theory (DFT)[29, 30]. The localized impurities, which are determined by the on-site Coulomb interaction, can be correctly described by the non-perturbative theory, such as the Hirsch–Fye quantum Monte Carlo (QMC) technique[31].

In order to accurately describe these two kinds of objects in real materials by a unified theoretical framework, we proposed a combined DFT + QMC method. First, the one-particle parts of the Anderson impurity model are formulated within the DFT or tight-binding approximation for determining the host band structure and the impurity-host hybridization. Second, the correlation parts of the Anderson impurity model at finite temperatures are calculated by the QMC method. For the case of singlet impurity, we can calculate the impurity bound state in the band gap, the magnetic susceptibility, the occupations number, the impurity-host magnetic correlations. For the case of multi-impurities, we can calculate the magnetic correlations between any orbitals and any positions of impurities. Our combined DFT + QMC method has been applied for designing functional semiconductors[19–21] and metals[32–34].

The Anderson impurity model[35] is defined as:

$$H = \sum_{\boldsymbol{k},\alpha,\sigma} [\epsilon_\alpha(\boldsymbol{k}) - \mu] c^\dagger_{\boldsymbol{k}\alpha\sigma} c_{\boldsymbol{k}\alpha\sigma}$$
$$+ \sum_{\boldsymbol{k},\alpha,i,\xi,\sigma} (V_{i\xi\boldsymbol{k}\alpha} d^\dagger_{i\xi\sigma} c_{\boldsymbol{k}\alpha\sigma} + h.c.)$$
$$+ (\varepsilon_d - \mu) \sum_{i,\xi,\sigma} d^\dagger_{i\xi\sigma} d_{i\xi\sigma} + U \sum_{i,\xi} n_{i\xi\uparrow} n_{i\xi\downarrow}. \quad (1)$$

$c^\dagger_{\boldsymbol{k}\alpha\sigma}$ and $c_{\boldsymbol{k}\alpha\sigma}$ are the creation and annihilation operators for host electrons, respectively. $\boldsymbol{k}$ is wave vector, and σ is spin of host electrons. $\alpha = v$ denotes valence band, and $\alpha = c$ the conduction band. $\epsilon_\alpha(\boldsymbol{k})$ is host electron band. μ is chemical potential. $d^\dagger_{i\xi\sigma}$ and $d_{i\xi\sigma}$ are the creation and annihilation operators of impurity localized electron, respectively. Impurity site is i, orbital is ξ, and spin is σ. Impurity occupation number is defined as $n_{i\xi\sigma} = d^\dagger_{i\xi\sigma} d_{i\xi\sigma}$. Hybridization between the impurity and the host is $V_{i\xi\boldsymbol{k}\alpha}$. The energy level of impurity 3d

orbital is ε_d. The on-site Coulomb repulsion of the impurity is U. The single-orbital approximation is used, i.e. Hund coupling J_H is neglected, to describe the magnetic sates of impurities.

The hybridization matrix element between the impurity and the host is expressed as $V_{i\xi\boldsymbol{k}\alpha} \equiv \langle \varphi_\xi(\boldsymbol{i}) | H | \Psi_\alpha(\boldsymbol{k}) \rangle \equiv \frac{1}{\sqrt{N}} e^{i\boldsymbol{k}\cdot\boldsymbol{i}} V_{\xi\alpha}(\boldsymbol{k})$, which can be obtained as

$$V_{\xi\alpha}(\boldsymbol{k}) = \sum_{o,n} e^{i\boldsymbol{k}\cdot(\boldsymbol{n}-\boldsymbol{i})} a_{\alpha o}(\boldsymbol{k}) \langle \varphi_\xi(\boldsymbol{i}) | H | \varphi_o(\boldsymbol{n}) \rangle. \quad (2)$$

$\varphi_\xi(\boldsymbol{i})$ is impurity $3d$ state at site $\boldsymbol{i}$. $\Psi_\alpha(\boldsymbol{k})$ is host state with band index α and wave vector $\boldsymbol{k}$. It is expanded by atomic orbitals $\varphi_o(\boldsymbol{n})$ with orbital index o, site index $\boldsymbol{n}$, expansion coefficient $a_{\alpha o}(\boldsymbol{k})$. Total number of host lattice sites is N. To calculate the matrix element $\langle \varphi_\xi(\boldsymbol{i}) | H | \varphi_o(\boldsymbol{n}) \rangle$, the DFC calculation based on a supercell is needed.

With parameters obtained by DFT calculations, magnetic correlations of the impurities can be calculated using the Hirsch-Fye QMC technique. The operators of z component of magnetic moment $M^z_{i\xi}$ and impurity occupation number n_ξ are defined, respectively,

$$M^z_{i\xi} = n_{i\xi\uparrow} - n_{i\xi\downarrow}, \quad (3)$$

$$n_{i\xi} = n_{i\xi\uparrow} + n_{i\xi\downarrow}, \quad (4)$$

where ξ is orbital of impurity, $\boldsymbol{i}$ is impurity site, $\uparrow$ is spin-up, and $\downarrow$ is spin-down.

3. Diluted magnetic semiconductors with wide band gaps

3.1. (Zn,Mn)O

As an example of diluted magnetic semiconductors with wide band gaps, we discuss the ferromagnetism in the compound Mn-doped ZnO[19].

For ZnO, the wurtzite structure is the most common phase. In thin films, the zincblende structure is stable. At high pressure, the rocksalt structure is also experimentally possible. The band structures of ZnO with the wurtzite, zinc-blende, and rocksalt structures can be calculated using the tight-binding parameters, as shown in Figs. 2(a)–2(c), respectively. For the wurtzite and zincblende structures, a direct gap of 3.45 eV is obtained. For the rocksalt structure, an indirect semiconductor gap is obtained.

For Mn-doped ZnO, the hybridization parameter $V_{\xi\alpha}(k)$ between the Mn impurity and the host Zn is plotted in Fig. 3. It is noted that the hybridization vanish at the Γ point for the rocksalt structure, and hybridization value at the Γ point for zincblende structure is larger than that for wurtzite structure.

Figs. 4(a) and 4(b) shows square of the magnetic moment at the impurity site $\langle (M^z)^2 \rangle$ as a function of chemical potential μ for Mn-doped in ZnO. The presence of a discontinuity in $\langle (M^z)^2 \rangle$ versus μ are observed, which denotes the existence of an impurity bound state (IBS) at this energy. For (Zn,Mn)O, the shallow IBS with position $\omega^Z_{IBS} \approx 0.1$ eV and $\omega^W_{IBS} \approx 0.2$ eV are obtained for the zinblende and wurtzite structures, respectively. A much deeper IBS with position $\omega^R_{IBS} \approx 1.6$ eV is found
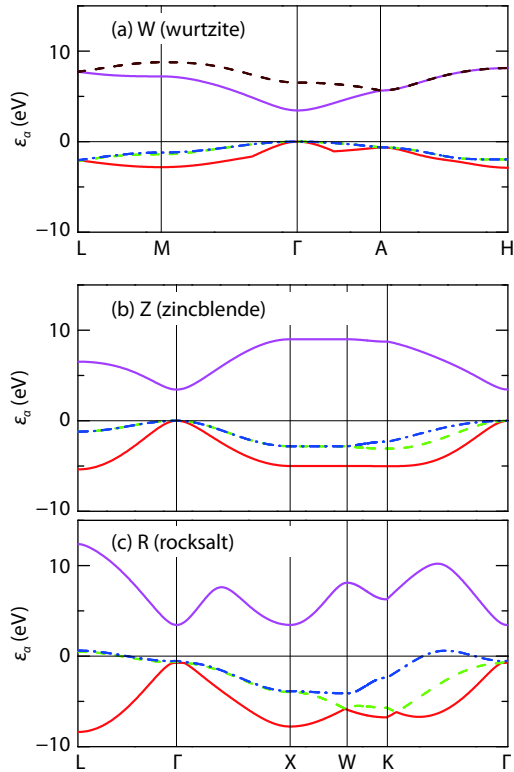
Fig. 2. (Color online) Band structure of the ZnO host with wurtzite, zincblende, and rocksalt crystal structures. Adapted from Ref. [19].
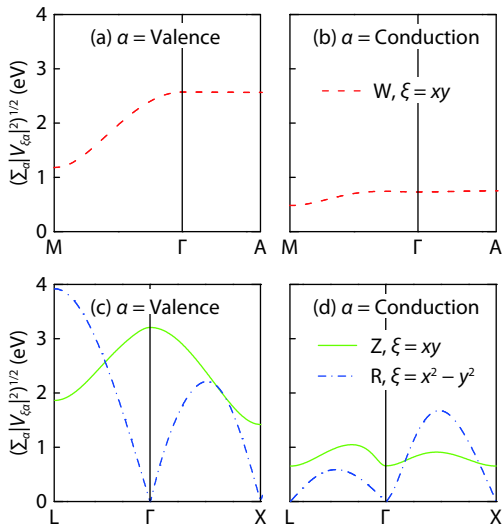

Fig. 3. (Color online) For Mn impurity in ZnO, hybridization parameter $V_{\xi\alpha}(k)$ of a Mn ξ orbital with the valence bands and the conduction bands. Adapted from Ref. [19].
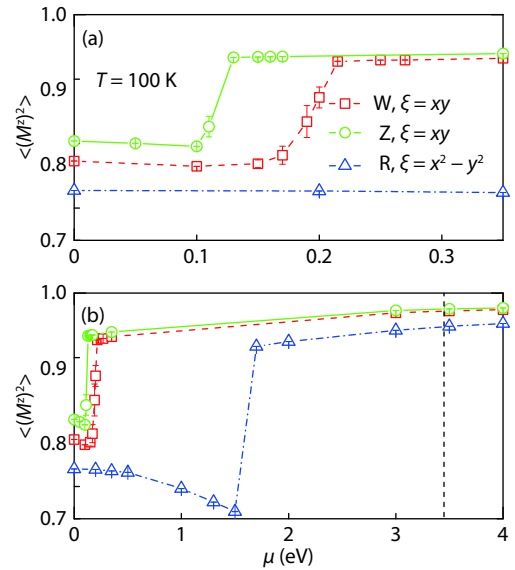

Fig. 4. (Color online) For Mn impurity in ZnO, square of the magnetic moment at the impurity site $\langle (M^z)^2 \rangle$ as a function of the chemical potential μ. The top of valence is energy zero, and the bottom of the conduction band is noted as vertical dashed lines. Adapted from Ref. [19].
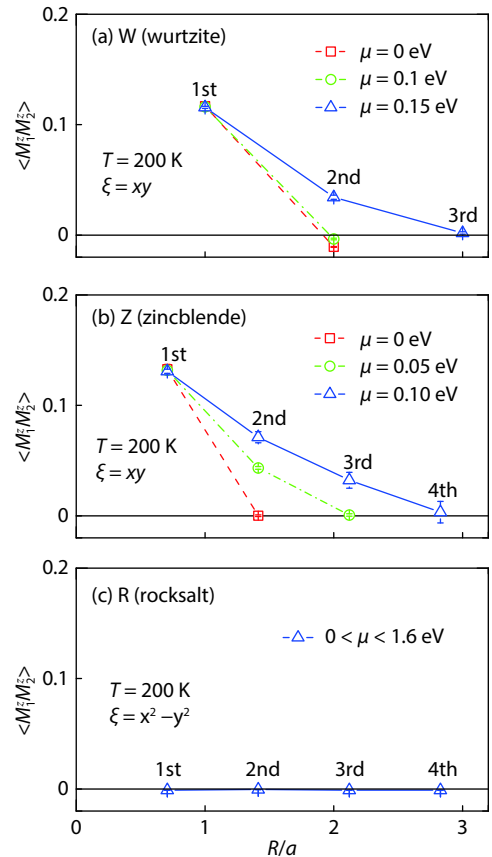

Fig. 5. (Color online) For Mn impurity in ZnO, impurity-impurity magnetic correlation function $\langle M_1^z M_2^z \rangle$ as a functino of distance R between two impurities for the wurtzite, zincblende, and rocksalt structures. a is lattice constant. Adapted from Ref. [19].

with rocksalt structure. In addition, no IBS is found near the bottom of conduction band for all three structures.

Impurity–impurity magnetic correlation function $\langle M_1^z M_2^z \rangle$ as a function of impurity separation R is shown in Fig. 5. a is the lattice constant. For wurtzite structure, ferromagnetic correlation between Mn impurities is obtained with chemical potential $\mu = 0.0$. The range of the ferromagnetic correlation becomes longer with $\mu = 0.15$ eV. Ferromagnetic correlations becomes weaker with further increasing μ. Similar results are obtained for the zincblende structure, as shown in Fig. 5(b). A longer range of ferromagnetic correlations is obtained in

zincblende structure than that in wurtzite structure. No magnetic correlations is obtained for the rocksalt structure, as shown in Fig. 5(c). This is due to the fact that the IBS of rocksalt structure is too deep, as seen in Fig. 4. These results show that, for
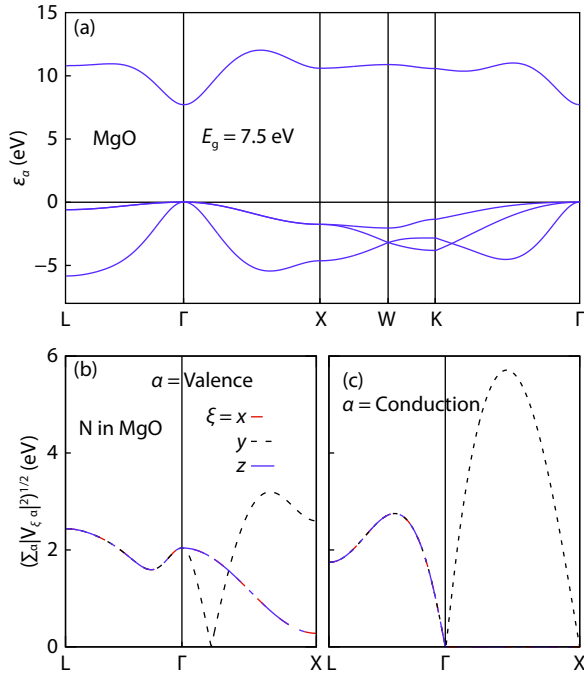
Fig. 6. (Color online) For N impurity in MgO, host band and hybridization. (a) MgO bands structure, where an direct band gap of 7.5 eV was obtained. Hybridization between $2p$ orbitals of N and (b) valence bands and (c) conduction bands of MgO. Adapted from Ref. [21].
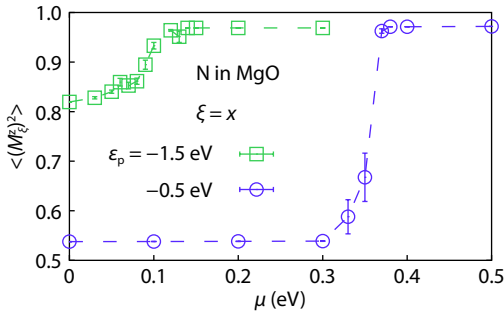

Fig. 7. (Color online) For N impurity in MgO, square of magnetic moment $\langle (M_\xi^z)^2 \rangle$ as a function of chemical potential μ. Adapted from Ref. [21].

shallow IBS, the ferromagnetic interaction between impurities can be obtained as the condition $\mu \sim \omega_{\text{IBS}}$ is satisfied.

3.2. d^0 type Mg(O,N)

As another example of diluted magnetic semiconductors with wide band gap, we discuss the ferromagnetism in the compound N-doped MgO, which is the so-called d^0 magnetic semiconductors [21].

MgO has a rocksalt structure. The band structure of MgO is shown in Fig. 6(a). The bottom of conduction band is dominated by $3s$ orbital of Mg, and the top of valence bands mainly comes from the $2p$ orbitals of O. At the Γ point, a very wide band gap of 7.5 eV is obtained.

The hybridization at the Γ point between ξ orbital of N impurity and valence bands of MgO is finite, while that with conduction band is zero. Since the gap edge of MgO is at Γ point, the hybridization value near Γ will be important. Due to the mixing between impurity and host, an impurity bound state may appear in the gap.
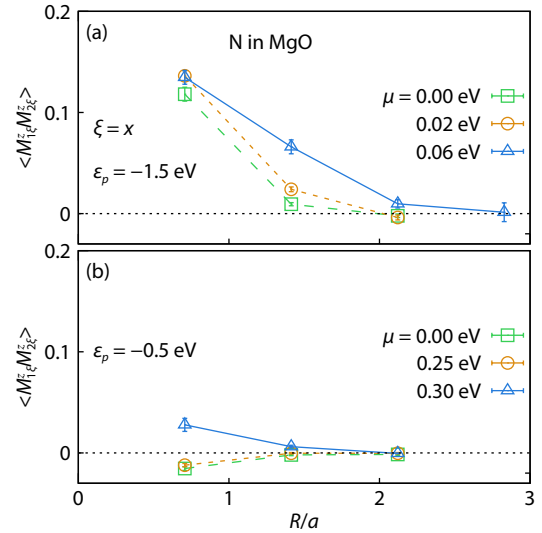

Fig. 8. (Color online) For N impurity in MgO, impurity-impurity magnetic correlation $\langle M_{1\xi}^z M_{2\xi}^z \rangle$ as a function of distance R, for the impurity level (a) $\epsilon_p = -1.5$ eV and (b) $\epsilon_p = -0.5$ eV. Adapted from Ref. [21].

The square of magnetic moment $\langle (M_\xi^z)^2 \rangle$ as a function of chemical potential μ is shown in Fig. 7. Sharp increases in the magnitude of $\langle (M_\xi^z)^2 \rangle$ are observed, around the energy of 0.08 eV for the impurity $2p$ energy $\epsilon_p = -1.5$ eV, and around the energy of 0.35 eV for $\epsilon_p = -0.5$ eV. Near the bottom of the conduction band, no such sharp variation is observed. As shown in Fig. 6, the hybridization with conduction band are around zero at Γ, much weaker than the hybridization with valence bands. The IBS is expected at the energy of sharp increase (or decrease) in $\langle (M_\xi^z)^2 \rangle$ as a function of μ.

The magnetic correlation function $\langle M_1^z M_2^z \rangle$ of $\xi = x$ orbitals of N as a function of impurity separation R is studied, and the results are shown in Fig. 8. a is lattice constant. For impurity energy $\epsilon_p = -1.5$ eV, ferromagnetic correlations are obtained at chemical potential $\mu = 0.0$ eV. For $\epsilon_p = -1.5$ eV, the IBS lies about 0.08 eV in the gap, as shown in Fig. 7. For μ to 0.06 eV, ferromagnetic correlations become larger and longer. These results confirmed that, like what we obtained in Mn-doped ZnO case, for shallow IBS the ferromagnetic interaction between impurities can develop as the condition $\mu \sim \omega_{\text{IBS}}$ is satisfied.

4. Diluted magnetic semiconductors with narrow band gaps

4.1. Ba(Zn,Mn)$_2$As$_2$

As an example of diluted magnetic semiconductors with narrow band gaps, we discuss the ferromagnetism in the compound Mn-doped BaZn$_2$As$_2$ [17].

By using the Wien2k package[36], we calculate the band structure $\epsilon_\alpha(k)$ and hybridization parameters $V_{i\xi k\alpha}$, as shown in Fig. 9. By the modified Beck–Johnson exchange potential (mBJ) [37], the gap band $E_g = 0.2$ eV is obtained. It is consistent with previous calculations[14, 38] and experimental value[11].

For Mn impurity in BaZn$_2$As$_2$, the impurity occupation number $\langle n_\xi \rangle$ as a function of chemical potential μ is shown in Fig. 10(a). The top of valence band is set as 0, and the bottom
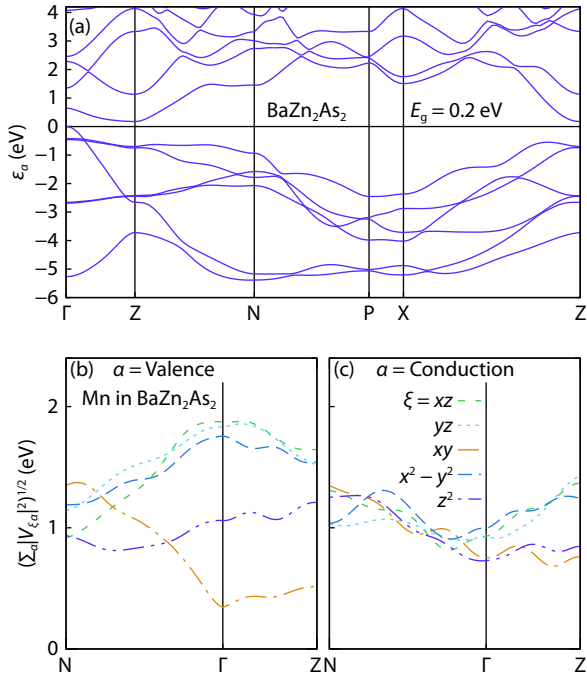
Fig. 9. (Color online) For Mn impurity in $BaZn_2As_2$, host band and impurity-host hybridization. (a) Energy bands off host $BaZn_2As_2$. Band gap of 0.2 eV was obtained by DFT calculations, consistent with experiment[11]. The hybridization parameter between the $3d$ orbitals of Mn and (b) valence bands and (c) conduction bands of $BaZn_2As_2$. Adapted from Ref. [17].
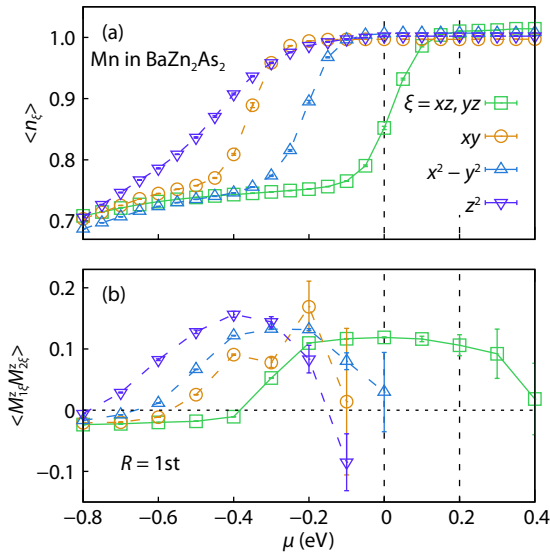

Fig. 10. (Color online) For Mn impurity in $BaZn_2As_2$, chemical potential μ dependence of (a) impurity occupation number $\langle n_\xi \rangle$ of ξ, and (b) magnetic correlation $\langle M_{1\xi}^z M_{2\xi}^z \rangle$ between impurities of the first-nearest neighbor. The band gap of 0.2 eV is noted by dash lines. Adapted from Ref. [17].

of conduction band is set as 0.2 eV. Sharp increases in n_ξ are observed. For the orbitals $\xi = z^2, xy, x^2 - y^2$, and $xz(yz)$, the IBS exists at energy $\omega_{\mathrm{IBS}} = -0.5, -0.4, -0.2$, and 0.0 eV, respectively. Magnetic correlation $\langle M_{1\xi}^z M_{2\xi}^z \rangle$ between impurities of the first-nearest neighbor is shown in Fig. 10(b).

For Mn impurities in $BaZn_2As_2$, we study the magnetic correlation $\langle M_{1\xi}^z M_{2\xi}^z \rangle$ as a function of the distance R. For p-type
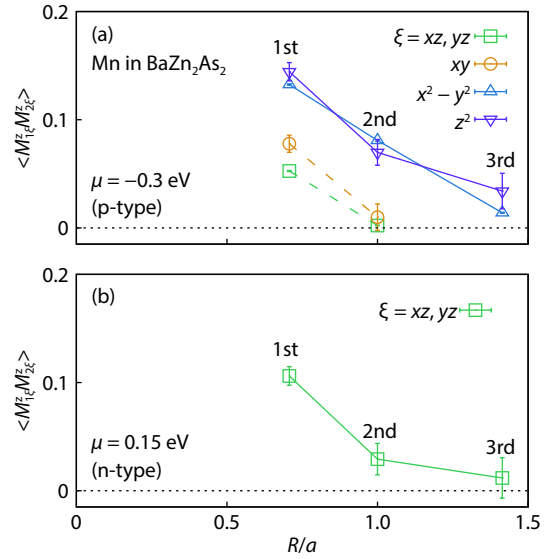

Fig. 11. (Color online) For Mn impurities in $BaZn_2As_2$, magnetic correlation $\langle M_{1\xi}^z M_{2\xi}^z \rangle$ as a function of distance R. (a) Chemical potential is set as $\mu = -0.3$ eV to model p-type case. (b) It is set as $\mu = 0.15$ eV for n-type case. The first, second, and third nearest neighbors of R are noted. Adapted from Ref. [17].

carriers, we take $\mu = -0.3$ eV as shown in Fig. 11(a). Long-range ferromagnetic coupling is obtained for the orbitals $\xi = x^2 - y^2$ and z^2. For n-type n-type carriers, we take $\mu = 0.15$ eV as shown in Fig. 11(b). Long-range ferromagnetic coupling is obtained for the orbitals $\xi = xz$ and yz. It is observed that the ferromagnetic interaction between impurities can develop as the condition $\mu - \omega_{\mathrm{IBS}}$ is satisfied, when IBS is close to the band edges.

4.2. Ba(Zn,Cr)$_2$As$_2$

As other example of magnetic semiconductor with narrow band gap, we discuss the ferromagnetism in the compound Cr-doped $BaZn_2As_2$[18].

In host $BaZn_2As_2$, let us compare the ferromagnetic coupling due to Cr impurities and that due to Mn impurities. The position of IBS of Cr impurity is closer to the bottom of the conduction band than that of the Mn impurity, as shown in Fig. 12(a). This is reasonable, since the energy level of Cr impurity is higher than that of the Mn impurity. The magnetic correlation $\langle M_{1\xi}^z M_{2\xi}^z \rangle$ between two impurities with the 1st nearest neighbor is shown in Fig. 12(b). For n-type carrier with $\mu \sim 0.2$ eV, the ferromagnetic correlation for the Cr impurity is expected. It is more promising than that for the Mn impurity.

For Cr impurities in $BaZn_2As_2$, we study the magnetic correlation $\langle M_{1\xi}^z M_{2\xi}^z \rangle$ as a function of the distance R. For p-type carriers, we take $\mu = -0.1$ eV as shown in Fig. 13(a). Long-range ferromagnetic coupling is obtained for the orbital $\xi = x^2 - y^2$. For n-type carriers, we take $\mu = 0.15$ eV as shown in Fig. 13(b). Long-range ferromagnetic coupling is obtained for the orbitals $\xi = xz$ and yz. It is observed that the ferromagnetic interaction between impurities can develop as the condition $\mu \sim \omega_{\mathrm{IBS}}$ is satisfied, for both p- and -type carriers.

5. Two-dimensional magnetic semiconductors

5.1. Cr$_2$Ge$_2$Se$_6$
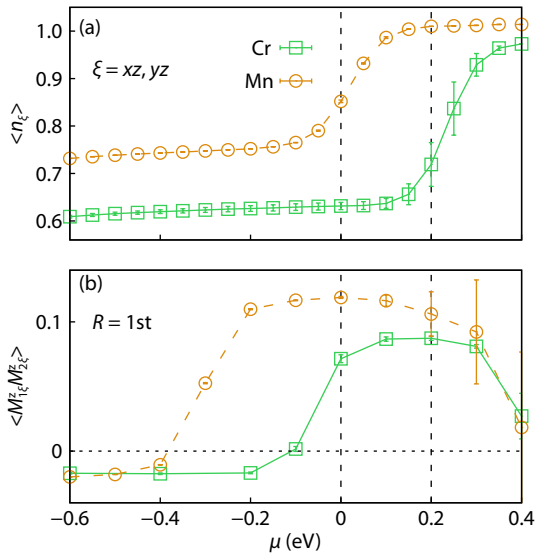
As an example of 2D magnetic semiconductors, we dis-

Fig. 12. (Color online) Cr impurity versus Mn impurity in host $BaZn_2As_2$. Chemical potential μ dependence of (a) impurity occupation number $\langle n_\xi \rangle$, and (b) magnetic correlation $\langle M_{1\xi}^z M_{2\xi}^z \rangle$ between impurities of the 1st nearest neighbor. Adapted from Ref. [18].
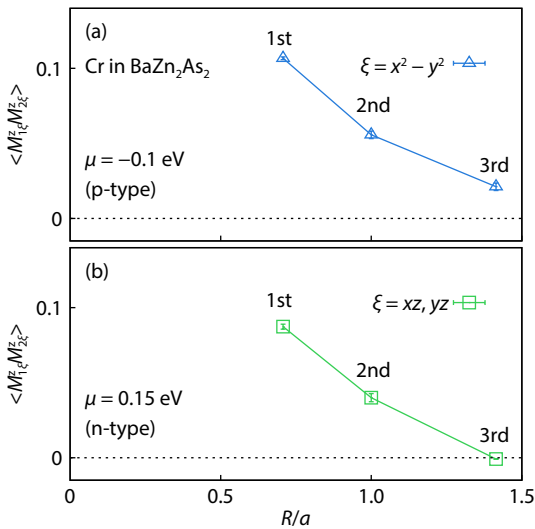

Fig. 13. (Color online) For Cr impurity in $BaZn_2As_2$, magnetic correlation $\langle M_{1\xi}^z M_{2\xi}^z \rangle$ as a function of the distance R. (a) chemical potential is set as $\mu = -0.1$ eV to model p-type case. (b) It is set as $\mu = 0.15$ eV for n-type case. The first, second, and third nearest neighbors of R are noted. Adapted from Ref. [18].

cussed our recent work on $Cr_2Ge_2Te_6$, which was predicted to have room temperature T_c by applying a few percent strain[39].

The structure of the $Cr_2Ge_2Se_6$ monolayer is depicted in Fig. 14, whose space group is $P\bar{3}1m$ (No.162). The band structure of $Cr_2Ge_2Se_6$ is obtained by DFT calculation, as shown in Fig. 15. A band gap of 0.748 eV is observed.

For monolayer $Cr_2Ge_2Se_6$, the normalized magnetization as a function of temperature is obtained by the Monte Carlo simulation and the DFT calculation, as shown in Fig. 16. The calculated Curie temperature for 2D $Cr_2Ge_2Se_6$ is $T_c = 144$ K. The Curie temperature can be enhanced to $T_c = 326$ K by applying 3% tensile strain, and $T_c = 500$ K with 7% tensile strain, as shown in Fig. 16. For 3% tensile strain, the volume cell increases 9%. Our result predicts that 2D $Cr_2Ge_2Se_6$ by applying
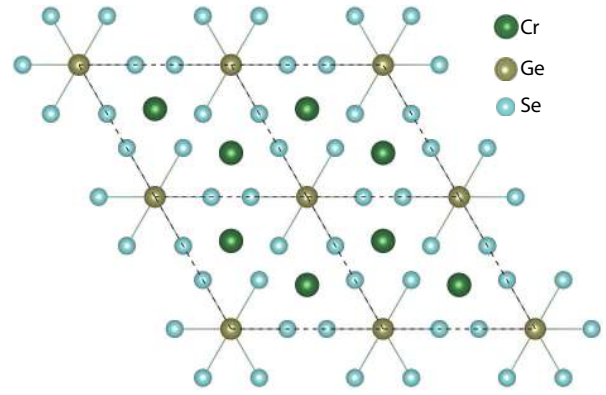

Fig. 14. (Color online) Crystal structure of two-dimensional $Cr_2Ge_2Se_6$.
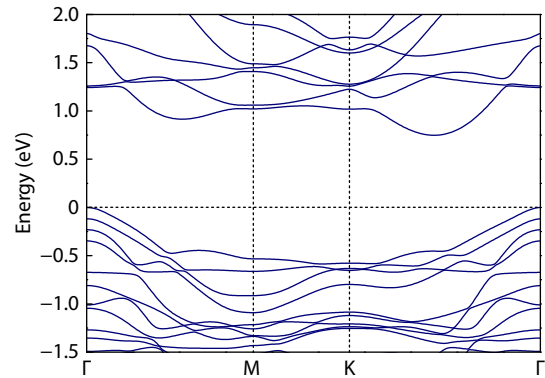

Fig. 15. (Color online) Electron band structure of two-dimensional $Cr_2Ge_2Se_6$, obtained by the density functional theory calculations. Adapted from Ref. [39].
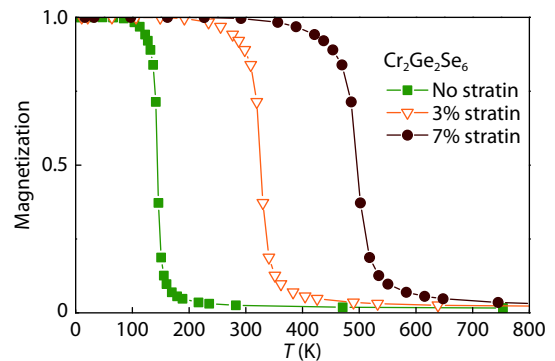

Fig. 16. (Color online) For two-dimensional $Cr_2Ge_2Se_6$ with different tensile strains, the normalized magnetization as a function temperature. Adapted from Ref. [39].

ing a few percent strain can be a promising candidate for room-temperature ferromagnetic semiconductor.

5.2. PtBr$_3$

As another example of 2D magnetic semiconductors, we discussed our recent work on $PtBr_3$, which was predicted to have room temperature T_c with quantum anomalous Hall effect (QAHE) [40].

$PtBr_3$ monolayer has space group $P\bar{3}1m$ (No.162), and the structure is depicted in Fig. 17. Due to crystal field, the d orbitals Pt are split into threefold t_{2g} and twofold e_g orbitals, where energy of e_g orbitals is higher than that of t_{2g} orbitals. Pt3+ has seven 5d electrons, six electrons occupied t_{2g} orbitals, and one fill e_g orbitals. So, spin at Pt site is $S = 1/2$.
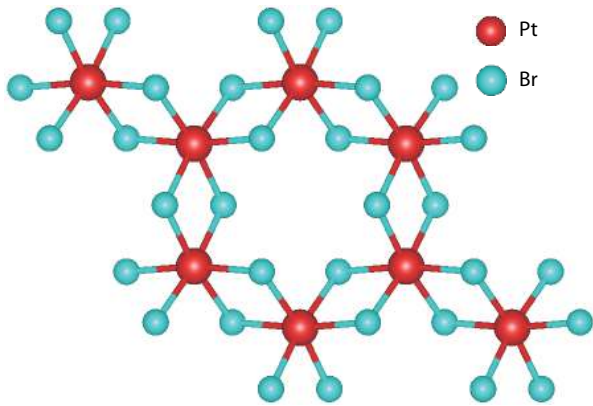
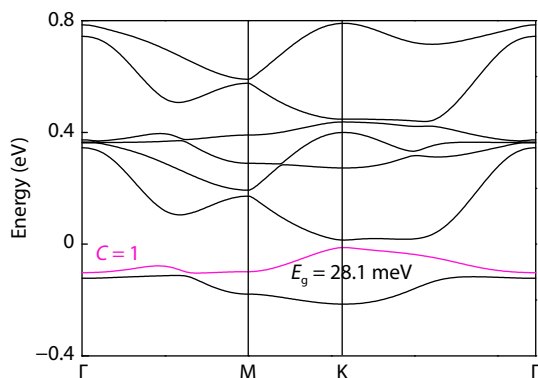Fig. 17. (Color online) Crystal structure of two-dimensional PtBr$_3$.

Fig. 18. (Color online) The band structure of two-dimensional PdBr$_3$, where Chern number C of the nontrivial band near Fermi energy E_F is indicated, and the band gap is $E_g = 28.1$ meV. The result is obtained by the density functional theory calculation. Adapted from Ref. [40].
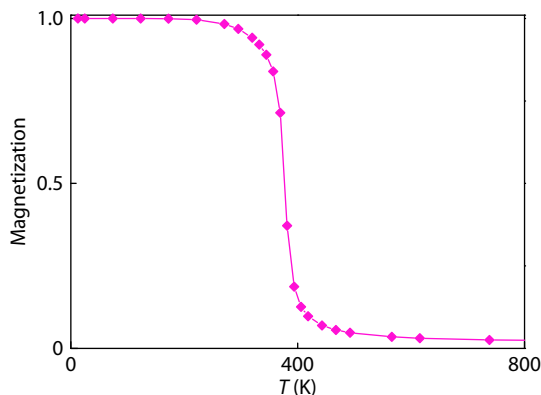

Fig. 19. (Color online) For two-dimensional PtBr$_3$, temperature dependence of the normalized magnetic moment obtained by the Monte Carlo simulation and the density functional theory calculation. Adapted from Ref. [40].

The band structure of PtBr$_3$ monolayers is calculated by the DFT method, as shown in Fig. 18. A band gap $E_g = 28.1$ meV is obtained for PtBr$_3$ monolayer due to the spin-orbit coupling. E_g/k_B is higher than room temperature. On the other hand, topologically nontrivial band structure is characterized by a nonzero Chern number C, which counts the number of edge states. For the band just below the Fermi level, its Chern number C obtained by integrating the Berry curvature over the BZ is 1, as shown by a line with red color in Fig. 18.

For monolayer PtBr$_3$, the normalized magnetization as a function of temperature is obtained by the Monte Carlo simulation and the DFT calculation, as shown in Fig. 19. The calculated Curie temperature for 2D PtBr$_3$ is $T_c = 375$ K. Since the QAHE is expected due to the coexist of nonzero Chern number and ferromagnetism, the 2D PtBr$_3$ can be potential candidates with QAHE at room temperature.

6. Discussions

In 2016, an experimental team obtained a Curie temperature higher than room temperature in Fe-doped p-type semiconductor GaSb[41]. On the other hand, the ferromagnetic semiconductor with n-type carriers has also been reported in recent experimental progress. In 2017, n-type semiconductor material Ba (Zn,Co)$_2$As$_2$ sith $T_c = 45$ K was reported in experiment[16]. In 2017, two experiment groups[42, 43] reported that Curie temperature higher than room temperature was obtained in Fe doped n-type semiconductor InSb. In 2018, an experimental team reported using electric fields to control Curie temperature in Fe doped n-type semiconductor InSb[44]. A common feature of these magnetic semiconductor materials with high Curie temperature is that the energy gap of the parent semiconductors is very small, in line with the direction of the magnetic semiconductors with narrow energy gap proposed by us in 2016[17]. The study of this direction has just started, and it is urgent to further study the repeatability of experiments, the comparison of theory and experiment, the analysis of the fine electronic properties and magnetic properties of existing materials, and the development of new materials.

The 2D magnetic semiconductor materials, which have been reported in recent experiments, will undoubtedly greatly promote the development of magnetic semiconductors[45]. The research into 2D magnetic semiconductors is just in its infancy, and many problems need to be studied urgently, such as key material parameters affecting ferromagnetism, the topological properties of the system, the transport properties and so on. The 2D magnetic semiconductors are becoming a hot research topic, and show potential as a powerful application prospect.

References

[1] Maekawa S. Concepts in spin electronics. Oxford University Press, 2006
[2] Maekawa S, Valenzuela S O, Saitoh E, et al. Spin current. Oxford University Press, 2012
[3] Kenney D, Norman C. What don't we know. Science, 2005, 309, 75
[4] Ohno H. Making nonmagnetic semiconductors ferromagnetic. Science, 1998, 281, 951

[5] Dietl T. A ten-year perspective on dilute magnetic semiconductors and oxides. Nat Mater, 2010, 9, 965

[6] Chen L, Yang X, Yang F, et al. Enhancing the Curie temperature of ferromagnetic semiconductor (Ga,Mn)As to 200 K via nanostructure engineering. Nano Lett, 2011, 11, 2584

[7] Masek J, Kudrnovsky J, Maca F, et al. Dilute moment n-type ferromagnetic semiconductor Li(Zn,Mn)As. Phys Rev Lett, 2007, 98, 067202

[8] Deng Z, Jin C Q, Liu Q Q, et al. Li(Zn,Mn)As as a new generation ferromagnet based on a I–II–V semiconductor. Nat Commun, 2011, 2, 422

[9] Deng Z, Zhao K, Gu B, et al. Diluted ferromagnetic semiconductor Li(Zn,Mn)P with decoupled charge and spin doping. Phys Rev B, 2013, 88, 081203

[10] Ding C, Man H, Qin C, et al. $(La_{1-x}Ba_x)(Zn_{1-x}Mn_x)AsO$: A two-dimensional 1111-type diluted magnetic semiconductor in bulk form. Phys Rev B, 2013, 88, 041102

[11] Zhao K, Deng Z, Wang X C, et al. New diluted ferromagnetic semiconductor with Curie temperature up to 180 K and isostructural to the 122 iron-based superconductors. Nat Commun, 2013, 4, 1442

[12] Zhao K, Chen B J, Zhao G Q, et al. Ferromagnetism at 230 K in $(Ba_{0.7}K_{0.3})(Zn_{0.85}Mn_{0.15})_2As_2$ diluted magnetic semiconductor. Chin Sci Bull, 2014, 59, 2524

[13] Glasbrenner J K, Zutic I, Mazin I I. Theory of Mn-doped II–II–V semiconductors. Phys Rev B, 2014, 90, 140403

[14] Suzuki H, Zhao K, Shibata G, et al. Photoemission and X-ray absorption studies of the isostructural to Fe-based superconductors diluted magnetic semiconductor $Ba_{1-x}K_x(Zn_{1-y}Mn_y)_2As_2$. Phys Rev B, 2015, 91, 140401

[15] Suzuki H, Zhao G Q, Zhao K, et al. Fermi surfaces and p-d hybridization in the diluted magnetic semiconductor $Ba_{1-x}K_x(Zn_{1-y}Mn_y)_2As_2$ studied by soft X-ray angle-resolved photoemission spectroscopy. Phys Rev B, 2015, 92, 235120

[16] Guo S, Man H, Ding C, et al. $Ba(Zn,Co)_2As_2$: A diluted ferromagnetic semiconductor with n-type carriers and isostructural to 122 iron-based superconductors. Phys Rev B, 2019, 99, 155201

[17] Gu B, Maekawa S. Diluted magnetic semiconductors with narrow band gaps. Phys Rev B, 2016, 94, 155202

[18] Gu B, Maekawa S. New p- and n-type ferromagnetic semiconductors: Cr-doped $BaZn_2As_2$. AIP Adv, 2017, 7, 055805

[19] Gu B, Bulut N, Maekawa S. Crystal structure effect on the ferromagnetic correlations in ZnO with magnetic impurities. J Appl Phys, 2008, 104, 103906

[20] Ohe J, Tomoda Y, Bulut N, et al. Combined approach of density functional theory and quantum Monte Carlo method to electron correlation in dilute magnetic semiconductors. J Phys Soc Jpn, 2009, 78, 083703

[21] Gu B, Bulut, Ziman N T, et al. Possible d^0 ferromagnetism in MgO doped with nitrogen. Phys Rev B, 2009, 79, 024407

[22] Ichimura M, Tanikawa K, Takahashi S, et al. Foundations of quantum mechanics in the light of new technology. Edited by S Ishioka, K Fujikawa. Singapore: World Scientific, 2006, 183

[23] Bulut N, Tanikawa K, Takahashi S, et al. Long-range ferromagnetic correlations between Anderson impurities in a semiconductor host: Quantum Monte Carlo simulations. Phys Rev B, 2007, 76, 045220

[24] Tomoda Y, Bulut N, Maekawa S. Inter-impurity and impurity-host magnetic correlations in semiconductors with low-density transition-metal impurities. Physica B, 2009, 404, 1159

[25] Huang B, Clark G, Navarro-Moratalla E, et al. Layer-dependent ferromagnetism in a van der Waals crystal down to the monolayer limit. Nature, 2017, 546, 270

[26] Gong C, Li L, Li Z, et al. Discovery of intrinsic ferromagnetism in two-dimensional van der Waals crystals. Nature, 2017, 546, 265

[27] Bonilla M, Kolekar S, Ma Y, et al. Strong room-temperature ferromagnetism in VSe_2 monolayers on van der Waals substrates. Nat Nanotechnol, 2018, 13, 289

[28] O'Hara D J, Zhu T, Trout A H, et al. Room temperature intrinsic ferromagnetism in epitaxial manganese selenide films in the monolayer limit. Nano Lett, 2018, 18, 3125

[29] Hohenberg P, Kohn W. Inhomogeneous electron gas. Phys Rev, 1964, 136, B864

[30] Kohn W, Sham L J. Self-consistent equations including exchange and correlation effects. Phys Rev, 1965, 140, A1133

[31] Hirsch J E, Fye R M. Monte Carlo method for magnetic impurities in metals. Phys Rev Lett, 1986, 56, 2521

[32] Gu B, Gan J Y, Bulut N, et al. Quantum renormalization of the spin Hall effect. Phys Rev Lett, 2010, 105, 086401

[33] Gu B, Sugai I, Ziman T, et al. Surface-assisted spin Hall effect in Au films with Pt impurities. Phys Rev Lett, 2010, 105, 216401

[34] Xu Z, Gu B, Mori M, et al. Sign change of the spin Hall effect due to electron correlation in nonmagnetic CuIr alloys. Phys Rev Lett, 2015, 114, 017202

[35] Haldane F D M, Anderson P W. Simple model of multiple charge states of transition-metal impurities in semiconductors. Phys Rev B, 1976, 13, 2553

[36] Blaha P, Schwart K, Hadsen G K H, et al. WIEN2K, an augmented plane wave plus local orbitals program for calculating crystal properties. Vienna University of Technology, Vienna, 2001

[37] Tran F, Blaha P. Implementation of screened hybrid functionals based on the Yukawa potential within the LAPW basis set. Phys Rev B, 2011, 83, 235118

[38] Shein I R, Ivanovskii A L. Elastic, electronic properties and intra-atomic bonding in orthorhombic and tetragonal polymorphs of $BaZn_2As_2$ from first-principles calculations. J Alloys Compd, 2014, 583, 100

[39] Dong X J, You J Y, Gu B, et al. Strain-induced room-temperature ferromagnetic semiconductors with large anomalous Hall conductivity in two-dimensional $Cr_2Ge_2Se_6$. Phys Rev Appl, 2019, 12, 014020

[40] You J Y, Zhang Z, Gu B, et al. Two-dimensional room temperature ferromagnetic semiconductors with quantum anomalous Hall effect. arXiv: 1904.11357

[41] Tu N T, Hai P N, Anh L D, et al. High-temperature ferromagnetism in heavily Fe-doped ferromagnetic semiconductor (Ga,Fe)Sb. Appl Phys Lett, 2016, 108, 192401

[42] Tu N T, Hai P N, Anh L D, et al. A new class of ferromagnetic semiconductors with high Curie temperatures. arXiv: 1706.00735

[43] Kudrin A V, Danilov Y A, Lesnikov V P, et al. High-temperature intrinsic ferromagnetism in the (In,Fe)Sb semiconductor. J Appl Phys, 2017, 122, 183901

[44] Tu N T, Hai P N, Anh L D, et al. Electrical control of ferromagnetism in the n-type ferromagnetic semiconductor (In,Fe)Sb with high Curie temperature. Appl Phys Lett, 2018, 112, 122409

[45] Burch K S, Mandrus D, Park J G. Magnetism in two-dimensional van der Waals materials. Nature, 2018, 563, 47